A theoretical study of resonant tunnelling in the double-barrier structure

1989 J. Phys.: Condens. Matter 1 5451

(http://iopscience.iop.org/0953-8984/1/32/014)

J. Phys.: Condens. Matter 1 (1989) 5451–5461. Printed in the UK

A theoretical study of resonant tunnelling in the double-barrier structure

Jian-ping Peng†, Hao Chen†‡ and Shi-xun Zhou†

† Department of Physics, Fudan University, Shanghai, People's Republic of China

‡ International Centre for Theoretical Physics, 34100-Trieste, Italy

Received 2 August 1988, in final form 20 December 1988

Abstract. We present a theoretical study of resonant tunnelling in the double-barrier structure under the application of a constant electric field, based upon an exact solution of the Schrödinger equation. By using the transfer matrix technique, the transmission coefficient of the structure is determined as a function of the applied voltage and the incident electron energy. The current–voltage characteristics in the case of bulk carriers tunnelling into a two-dimensional quantum well and, for the first time, in the case of two-dimensional electrons tunnelling into a one-dimensional quantum wire are also calculated. The influence of the symmetry of the structure is studied. It is concluded that a larger peak-to-valley ratio can be expected by mere modulation of the width of the barrier.

1. Introduction

The study of resonant tunnelling in quantum well structures was pioneered by Tsu *et al* [1]. There has been renewed interest in it in the past few years, both experimentally and theoretically [2–13]. Devices based upon resonant tunnelling have found wide applications, such as photodetectors, transistors, light emitters and low-power logic circuits [2–13]. The most thoroughly studied material system as applied to double-barrier structures is the $GaAs/Al_{1-x}Ga_xAs$ system owing to the relative ease of its fabrication as well as its close lattice matching. Recently a double-barrier structure constructed of an ultrathin hydrogenated amorphous silicon (a-Si:H) layer sandwiched with hydrogenated amorphous stoichiometric silicon nitride ($a\text{-}Si_3N_4$:H) barriers has been fabricated successfully and electron resonant tunnelling has been observed [9].

Tsu *et al* first provided a theoretical description of the electron tunnelling in a finite superlattice [1]. Their calculation involves the solution of the Schrödinger equation in each region of the device under the assumptions that the applied bias is small, the effective mass is constant throughout, and phonon scattering can be neglected. They were able to correlate the energy location of the transmissivity peaks with the bound-state energies of the structure, and thus to attribute the negative resistance predicted by the current–voltage (I–V) plots to resonant tunnelling.

Recently, a theoretical study was presented in [15] of resonant tunnelling in a multi-layered heterostructure based on an exact solution of the Schrödinger equation under the application of a constant electric field. By use of the Airy function and the transfer

0953-8984/89/325451 + 11 $02.50

matrix technique, the transmissivity of the structure is determined as a function of the incident electron energy.

The effect of an applied electric field was considered in [16], and it was shown that with fully symmetrical barriers it leads to weaker resonances than otherwise possible. It is concluded that better structures can be designed to maximise resonance peaks but it is essential to take into account the effects of the field. Furthermore, because the field cancels the intrinsic simple symmetry, optimisation can only be performed for one of the possible several peaks.

The organisation of this paper is as follows. In § 2, we present calculations of the transmission coefficient as a function of the incident electron energy, and the energy of a selected peak as a function of the applied voltage; a comparison with those in [15] is given. In § 3, numerical considerations are presented of the effects of the electric field and the structural geometry on the transmission coefficient. In § 4 the *I–V* characteristics of the double-barrier structures are calculated for bulk carriers tunnelling into a two-dimensional well (i.e. the 3D–2D case) and for two dimensional electrons tunnelling into a one-dimensional quantum wire (i.e. the 2D–1D case). Finally, in § 5, some conclusions are drawn.

2. Calculations of the transmissivity

To calculate the transmission coefficient, the following assumptions have to be made first.

(i) The effective-mass approximation is valid and electrons are described by quadratic energy–momentum relations.

(ii) The electron mean free path is longer than the size of the double-barrier structure.

(iii) Conditions are such that the field pattern is uniform.

(iv) The effects of phonon scattering are negligible.

The Schrödinger equation of a particle in a uniform electric field has a solution which can be expressed as a linear combination of Bessel functions. So the calculation is performed by solving the Schrödinger equation exactly in each region and then matching the continuity of the wavefunction ψ and $(1/m)(\partial\psi/\partial x)$ for its derivative at each boundary [17–19].

A representative double-barrier structure with an applied bias is diagrammatically presented in figure 1(*b*). The solution in region 1 is simply a linear combination of an incident and a reflected plane wave:

$$\psi_1 = \exp(ikx) + R\exp(-ikx) \tag{1}$$

where $k = \sqrt{2m_a E/\hbar^2}$ and m_a is the effective mass in the well. With the following notation and transformation of variables

$$\lambda_b = (2m_b)^{1/3}(E - V_0)/(\hbar eF)^{2/3} \qquad \xi_b = x/L + \lambda_b$$

$$L = (\hbar^2/2m_b eF)^{1/3} \qquad z = (\tfrac{2}{3})|\xi_b|^{3/2}$$

the Schrödinger equation in region 2 can be written as

$$u''(z) + (1/z)u'(z) + [1 \pm (\tfrac{1}{3})^2/z^2]u(z) = 0 \tag{2}$$

where V_0 is the barrier height, m_b the effective mass in the barrier and $F =$

$V/(A_0 + B_{01} + B_{02})$ the electric field caused by the applied voltage V. When $\xi_b \geqslant 0$, the wavefunction can be written as

$$\psi_2 = \xi_b^{1/2}[C_2^+ J_{1/3}(z) + C_2^- Y_{1/3}(z)] \tag{3}$$

where $J_{1/3}$ and $Y_{1/3}$ are Bessel functions with order $\frac{1}{3}$ of the first kind and the second kind, respectively. When $\xi_b < 0$, the wavefunction can be written as

$$\psi_2 = |\xi_b|^{1/2}\{[-C_2^+ I_{1/3}(z) + C_2^-[(2/\pi)K_{1/3}(z) - \sqrt{3}\, I_{1/3}(z)]\} \tag{4}$$

where $I_{1/3}$ and $K_{1/3}$ are modified Bessel functions with order $\frac{1}{3}$ of the first kind and the second kind, respectively. The continuity of wavefunction and its derivative at $\xi_b = 0$ is now considered. Letting

$$B_2^+(x) = \begin{cases} \xi_b^{1/2} J_{1/3}(z) & \xi_b \geqslant 0 \\ -|\xi_b|^{1/2} I_{1/3}(z) & \xi_b < 0 \end{cases}$$

$$B_2^-(x) = \begin{cases} \xi_b^{1/2} Y_{1/3}(z) & \xi_b \geqslant 0 \\ |\xi_b|^{1/2}(2/\pi)K_{1/3}(z) - \sqrt{3}\, I_{1/3}(z) & \xi_b < 0 \end{cases}$$

the wavefunction has the following form:

$$\psi_2 = C_2^+ B_2^+(x) + C_2^- B_2^-(x). \tag{5}$$

Similarly, with the following notation and transformation of variables

$$\lambda_a = (2m_a)^{1/3} E/(\hbar e F)^{2/3} \qquad \xi_a = x/L + \lambda_a$$
$$L = (\hbar^2/2m_a eF)^{1/3} \qquad y = \tfrac{2}{3}\xi_a^{3/2}$$
$$y = (\tfrac{2}{3})\xi_a^{3/2}$$

the Schrödinger equation in region 3 can be written as

$$u''(y) + (1/y)u'(y) + [1 - (1/3)^2/y^2]u(y) = 0 \tag{6}$$

and the wavefunction as

$$\psi_3 = C_3^+ A_3^+(x) + C_3^- A_3^-(x) \tag{7}$$

where $A_3^+(x)$ and $A_3^-(x)$ are defined as

$$A_3^+(x) = \xi_a^{1/2} J_{1/3}(y) \qquad A_3^-(x) = \xi_a^{1/2} Y_{1/3}(y). \tag{8}$$

The wavefunction in region 4 has the same form as in region 2:

$$\psi_4 = C_4^+ B_2^+(x) + C_4^- B_2^-(x). \tag{9}$$

In region 5, only the transmission plane wave is included:

$$\psi_5 = \tau \exp(ik'x) \tag{10}$$

where $k' = \sqrt{2m_a(E + eV)/\hbar^2}$, V being the applied voltage.

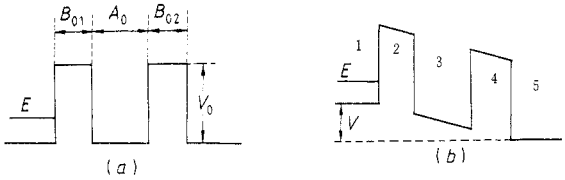

Figure 1. Potential energy diagram of a double-barrier structure: (*a*) no applied voltage; (*b*) with an applied voltage.

The boundary conditions at $x = 0$ gives [17–19]

$$\begin{aligned} 1 + R &= C_2^+ B_2^+(x=0) + C_2^- B_2^-(x=0) \\ (m_b/m_a)ik(1-R) &= C_2^+ B_2^{+\prime}(x=0) + C_2^- B_2^{-\prime}(x=0) \end{aligned} \tag{11}$$

which in matrix form becomes

$$\begin{bmatrix} 1 \\ R \end{bmatrix} = \frac{-1}{2ik}\begin{bmatrix} -ik & -1 \\ -ik & 1 \end{bmatrix}\begin{bmatrix} B_2^+(x=0) & B_2^-(x=0) \\ (m_a/m_b)B^{+\prime}(x=0) & (m_a/m_b)B^{-\prime}(x=0) \end{bmatrix}\begin{bmatrix} C_2^+ \\ C_2^- \end{bmatrix}. \tag{12}$$

Extending the analysis to other interfaces gives

$$\begin{bmatrix} 1 \\ R \end{bmatrix} = \frac{-1}{2ik}\begin{bmatrix} ik & -1 \\ -ik & 1 \end{bmatrix}\mathbf{S}\begin{bmatrix} 1 & 1 \\ ik' & -ik' \end{bmatrix}\begin{bmatrix} \tau \\ 0 \end{bmatrix} \tag{13}$$

where the matrix $\mathbf{S}$ is

$$\begin{aligned} \mathbf{S} = {} & \mathbf{S}_2(x=0)\mathbf{S}_2^{-1}(x=B_{01})\mathbf{S}_3(x=B_{01})\mathbf{S}_3^{-1}(x=A_0+B_{01}) \\ & \times \mathbf{S}_2(x=A_0+B_{01})\mathbf{S}_2^{-1}(x=A_0+B_{01}+B_{02}) \end{aligned} \tag{14}$$

and the matrices $\mathbf{S}_2(x)$ and $\mathbf{S}_3(x)$ are defined as

$$\mathbf{S}_2(x) = \begin{bmatrix} B_2^+(x) & B_2^-(x) \\ (m_a/m_b)B_2^{+\prime}(x) & (m_a/m_b)B_2^{-\prime}(x) \end{bmatrix} \qquad \mathbf{S}_3(x) = \begin{bmatrix} A_3^+(x) & A_3^-(x) \\ A_3^{+\prime}(x) & A_3^{-\prime}(x) \end{bmatrix}. \tag{15}$$

The transmission coefficient can be found as

$$T = \tau\tau^* = (4k/k')/[S_{11} + k'/kS_{22})^2 + (S_{21}/k - k'S_{12})^2] \tag{16}$$

where S_{12}, S_{11}, S_{21} and S_{22} are elements of the matrix $\mathbf{S}$.

The logarithm of the transmission coefficient as a function of the electron energy in a double-barrier structure made from GaAs/$Al_{1-x}Ga_xAs$ is presented in figure 2. Next we compare our results with the results obtained in [15]; the structure analysed and the boundary conditions used are identical with their case. The calculation is performed under two conditions.

(i) The masses in the well and two barriers are assumed to be equal to the GaAs mass: $m_a = m_b = 0.067\,m_0$.

(ii) Different masses in the layer are considered: $m_a = 0.067\,m_0$; $m_b = 0.1087\,m_0$.

The applied bias is 0.16 V. In figure 2, two resonant peaks appear in the transmission coefficient. The calculation is repeated at a higher voltage, 0.4 V, in figure 3. In this case, only one peak occurs in the transmission coefficient. The results show that the

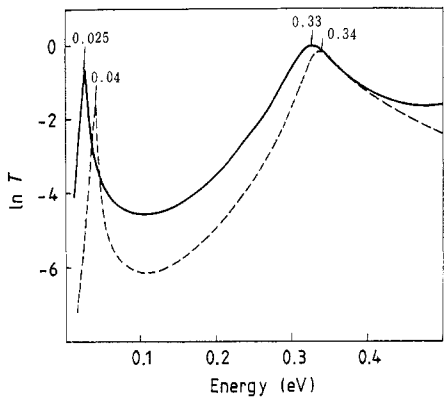

Figure 2. Logarithm of the transmission coefficient as a function of the incident electron energy at an applied bias of 0.16 V ($V_0 = 0.5$ eV; $B_{01} = B_{02} = 20$ Å; $A_0 = 50$ Å): ——, $m_a = 0.067m_0$, $m_b = 0.067m_0$; ---, $m_a = 0.067m_0$, $m_b = 0.1087m_0$.

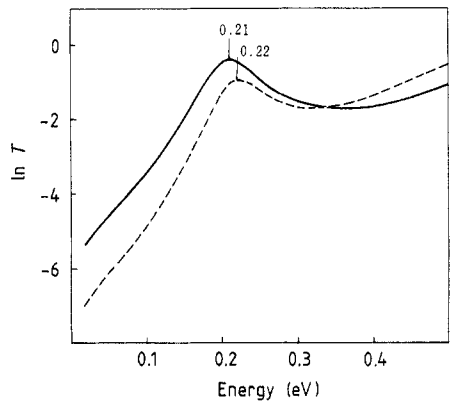

Figure 3. Logarithm of the transmission coefficient as a function of the incident electron energy at an applied bias of 0.4 V. ($V_0 = 0.5$ eV; $B_{01} = B_{02} = 20$ Å; $A_0 = 50$ Å): ——, $m_a = 0.067m_0$, $m_b = 0.067m_0$; ---, $m_a = 0.067m_0$, $m_b = 0.1087m_0$.

resonant energies are shifted upwards in the two-mass model from those calculated using the one-mass model.

We compare our calculated transmission coefficients with those in [15]. From figures 2 and 3, it can be seen that the results here differ from those in [15] in that there is not so much fine structure and there are small deviations in the locations of the transmission coefficient peaks. Even though different methods may yield small differences in the numerical results, our calculated curves of transmission coefficient are quite smooth and do not contain small lumps and bumps apart from the resonant peaks. We strongly believe that the results in [15] must be incorrect. As the limit of V approaches zero, the transmissivity should be the same as that calculated in [1] which is clearly a smooth function of the incident energy outside the resonant peaks or depends on the experimental data of the I–V characteristics which show that a negative differential resistance appears only at a voltage corresponding to a transmission coefficient peak [10, 12].

A plot of the energy of the lower-energy peak against the applied voltage is shown in figure 4. The higher the bias, the lower is the resonant energy because the conduction band bends under the action of the applied voltage. The lower-energy peak disappears when the applied voltage is greater than 0.2 V. Unexpectedly a linear relationship is obtained in our calculation, as shown in figure 4. Why this happens is an open question.

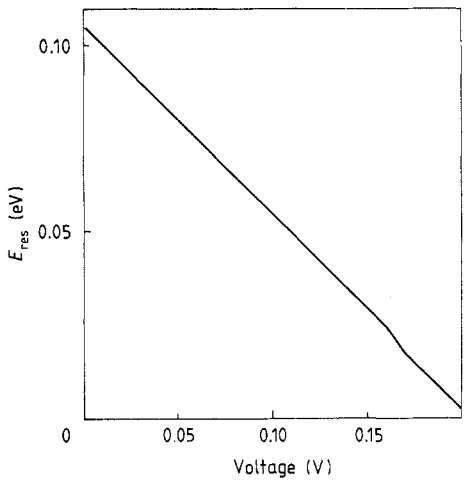

Figure 4. The resonant energy of the lower-energy peak as a function of the applied bias ($V_0 = 0.5$ eV; $B_{01} = B_{02} = 20$ Å; $A_0 = 50$ Å; $m_a = m_b = 0.067m_0$).

3. Effects of the structural symmetry

The effect of an applied electric field on the symmetry of the double-barrier structure was first considered in [16]. With the assumption of strong localisation, they showed that the resonant global transmission coefficient of a two-rectangle potential energy barrier becomes

$$T_{\text{Gres}} \simeq T_{\min}/T_{\max} \tag{17}$$

where $T_{\min}$ and $T_{\max}$ represent the smaller and the larger of the transmission coefficients of the left and the right barrier, respectively. Therefore, it can be concluded that, regardless of how small $T_{\min}$ and $T_{\max}$ are, the order of magnitude of the transmission coefficient T can be unity under the only condition $T_{\min} = T_{\max}$. In the absence of a field, with $B_{01} = B_{02}$ (as depicted in figure 1(a)), resonance would occur at energies satisfying

$$B_{01}\sqrt{2m^*E/\hbar^2} = 2\tan^{-1}[(V_0 - E)/E]^{1/2} + (n-1)\pi \tag{18}$$

because of the symmetry of the structure. These concepts were generalised in [16] to the general case of a double-barrier structure with an applied bias (as depicted in figure 1(b)). With the use of the WKB approximation the transmission coefficients of the left and the right barrier are, respectively,

$$\begin{aligned} T_l &= \exp[(-4/3\hbar)\sqrt{2m^*}(V_0^{3/2} - V_1^{3/2})/eF] \\ T_r &= \exp[(-4/3\hbar)\sqrt{2m^*}(V_2^{3/2} - V_3^{3/2})/eF] \end{aligned} \tag{19}$$

where V_0 is the barrier height

$$\begin{aligned} V_1 &= V_0 - eFB_{01} \\ V_2 &= V_0 - eF(B_{01} + A_{01}) \\ V_3 &= V_0 - eF(B_{01} + A_{01} + B_{02}) \end{aligned}$$

Since $T_l < T_r$ for $B_{01} = B_{02}$, we have

$$T_{\min}/T_{\max} = \exp[-(4/3\hbar)\sqrt{2m^*}(V_0^{3/2} - V_1^{3/2} - V_2^{3/2} + V_3^{3/2})/eF]. \tag{20}$$

Because the applied voltage destroys the symmetry of the barriers, the transmission

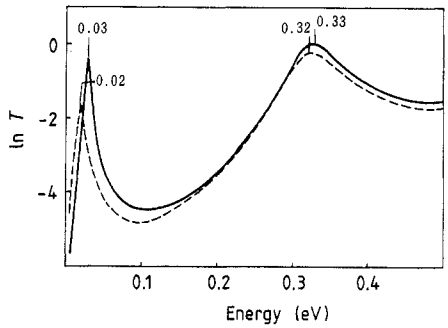

Figure 5. Logarithm of the transmission coefficient as a function of the electron energy for selected geometries at an applied bias of 0.16 V ($V_0 = 0.5$ eV; $A_0 = 50$ Å; $m_a = m_b = 0.067m_0$): ——, $B_{01} = 17$ Å; $B_{02} = 23$ Å; ---, $B_{01} = 23$ Å; $B_{02} = 17$ Å.

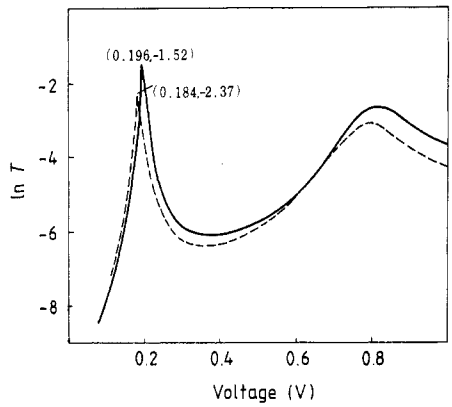

Figure 6. Logarithm of the transmission coefficient as a function of the applied voltage for selected geometries (electron energy $E = 0.005$ eV; $V_0 = 0.5$ eV; $A_0 = 50$ Å; $m_a = m_b = 0.067m_0$): ——, $B_{01} = B_{02} = 20$ Å; ---. $B_{01} = 23$ Å; $B_{02} = 17$ Å.

coefficients of the latter are no longer equal and lead to a drastic reduction in the effects at resonance with respect to the optimal possible condition. By use of a non-symmetrical structure with the left barrier thinner than the right barrier, the condition for $T_l = T_r$ might be recreated, thus enhancing the resonant tunnelling.

Figure 5 presents the logarithm of the transmission coefficient as a function of the electron energy for selected geometries, with the applied voltage being 0.16 V. For the full curve, asymmetry due to the width of the barrier cancels that from the effect of the applied voltage, and as a result the resonance is enhanced. Also the resonant energies can be seen to shift to higher energies when the left barrier is thinner than the right barrier.

Figure 6 shows the calculated transmission coefficient as a function of the applied voltage for selected geometries with the electron energy E being chosen to be 0.005 eV. The full curve is calculated for a symmetrical structure with the left barrier equal to the right barrier, while the broken curve is for a non-symmetrical structure with the left barrier thinner than the right barrier. A reduction in transmission coefficient is observable owing to the asymmetry due to the barrier width and to the electric field effect. The exact result of the transmission coefficient calculated here is larger by several orders of magnitude than that calculated in [16] using the WKB approximation.

4. Current–voltage characteristics

To calculate the current density, we first recall the dimensionality of resonant tunnelling in the double-barrier structure. In the most thoroughly studied structure, as originally proposed in [1], the current is controlled solely by the source-to-drain voltage and the bulk carriers tunnelling into two dimensional states in a quantum well (the 3D–2D case). In the new structure, as recently proposed in [8], the current is controlled not only by the source-to-drain voltage but also by the gate voltage. So the quantum well is linear rather than planar and the two-dimensional electrons tunnel into one-dimensional states

(the 2D–1D case). We refer to the source-to-drain voltage as the applied bias and the gate voltage has such a value that the two-dimensionality of the channel is sustained hereafter. It is obvious that the electron density is controlled by the gate voltage as well as being an intrinsic property of the material with which the structure is made.

Generally, the current density J may be computed as the average of the product of transmission coefficient T and the group velocity $\boldsymbol{v} = h^{-1}\nabla_k E$:

$$J = 2e/(2\pi)^d \int \mathrm{d}k^d \, V(k)T(E_t, E_l)[f(E) - f(E + eV)] \tag{21}$$

where $f(E) = [1 + \exp(E - E_F)/k_B\theta]^{-1}$ is the Fermi–Dirac distribution at the absolute temperature θ with E_F being the Fermi energy and k_B the Boltzmann constant. The dimensionality d is equal to 3 or to 2 for the 3D–2D and 2D–1D cases, respectively. The transverse components of J are zero by symmetry and, after a change in variable from momentum to energy, the longitudinal component becomes

$$J = \begin{cases} \dfrac{2m^*e}{(2\pi)^2\hbar^3} \displaystyle\int\int \mathrm{d}E_t \, \mathrm{d}E_l \, T(E_t, E_l)[f(E) - f(e + eV)] & \text{3D–2D case} \\ \dfrac{e\sqrt{m^*/8}}{\pi^2\hbar^2} \displaystyle\int\int \mathrm{d}E_t \, \mathrm{d}E_l \, T(E_t, E_l)[f(E) - f(e + eV)] & \text{2D–1D case} \end{cases} \tag{22}$$

In the 3D–2D case, the above expression for $\theta \to 0$ becomes

$$J = \begin{cases} \dfrac{2m^*e}{(2\pi)^2\hbar^3} \displaystyle\int_0^{E_F} (E_F - E_l)T(E_t, E_l) \, \mathrm{d}E_l & eV \geqslant E_F \\ \dfrac{2m^*e}{(2\pi)^2\hbar^3} \left(eV \displaystyle\int_0^{E_F - eV} T(E_t, E_l) \, \mathrm{d}E \right. & \\ \qquad \left. + \displaystyle\int_{E_F - eV}^{E_F} (E_F - E_l)T(E_t, E_l) \, \mathrm{d}E_l \right) & eV < E_F \end{cases} \tag{23}$$

and in the 2D–1D case for $\theta \to 0$ it becomes

$$J = \begin{cases} \dfrac{e\sqrt{m^*/8}}{\pi^2\hbar^2} \displaystyle\int_0^{E_F} (E_F - E_l)^{1/2} T(E_t, E_l) \, \mathrm{d}E_l & eV \geqslant E_F \\ \dfrac{e\sqrt{m^*/8}}{\pi^2\hbar^2} \left(\displaystyle\int_0^{E_F} (E_F - E_l)^{1/2} T(E_t, E_l) \, \mathrm{d}E_l \right. & \\ \qquad \left. - \displaystyle\int_0^{E_F - eV} (E_F - eV - E_l)^{1/2} T(E_t, E_l) \, \mathrm{d}E_l \right). & eV < E_F \end{cases} \tag{24}$$

The 3D–2D current density is the same as that obtained in [1]. It can be seen that the current density integration depends on the energy differently in different cases and is the main difference between the 3D–2D and the 2D–1D case.

Figures 7 and 8 show the calculated current density at zero temperature for a double-barrier structure in the 3D–2D and 2D–1D cases as a function of the applied voltage, respectively. Note that, in both cases, the current density shows an oscillatory behaviour as the applied voltage is increased. A maximum in current density, accompanied by a region of negative differential conductance, appears at a voltage when the quasi-eigen-energy in the well matches the Fermi energy of the electrons. Unexpectedly, the shapes

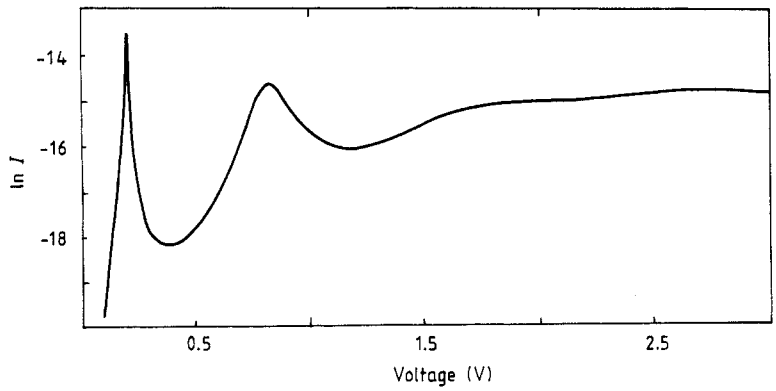

Figure 7. Logarithm of the 3D–2D current density $J(em^*/2\pi^2\hbar^3)^{-1}(1.6\times10^{-19})^2$ as a function of the applied voltage at zero temperature ($V_0 = 0.5$ eV; $B_{01} = B_{02} = 20$ Å; $A_0 = 50$ Å; $m_a = m_b = 0.067m_0$; $E_F = 0.005$ eV).

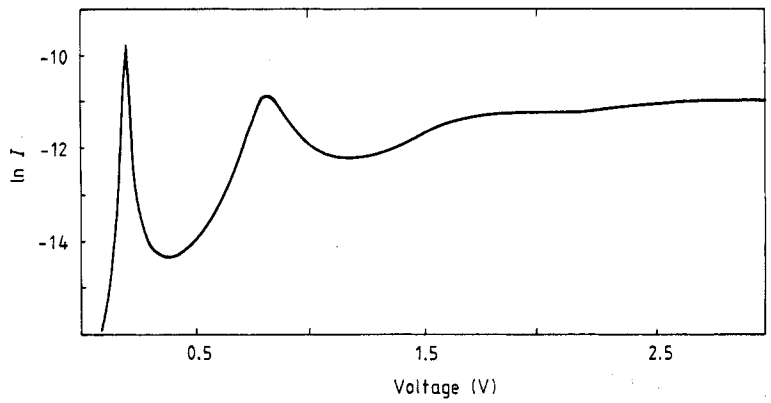

Figure 8. Logarithm of the 2D–1D current density $J(e\sqrt{m^*}/8/\pi^2\hbar^2)^{-1}(1.6\times10^{-19})^{3/2}$ as a function of the applied voltage at zero temperature ($V_0 = 0.5$ eV; $B_{01} = B_{02} = 20$ Å; $A_0 = 50$ Å; $m_a = m_b = 0.067m_0$; $E_F = 0.005$ eV).

of these two plots are almost identical with maxima and minima appearing at almost the same energies. This can be understood as follows. The expressions for J suggest that the shape of J against the applied voltage depends, on the competition between the voltage dependence of the transmission coefficient and that of the energy. In our computations, E_F is assumed to have a low value of 0.005 eV such that the transmission coefficient varies smoothly with energy as shown in figures 2 and 3.

In fact, as shown in figure 6, the transmission coefficient varies considerably with the applied voltage even at such low energies. Consequently, it can be expected that the I–V characteristic has approximately the same shape as that of the I–V curve. It is also expected that differences between the shapes of I–V characteristics for the 3D–2D and 2D–1D cases should be more pronounced at higher Fermi energies.

Figure 9 shows the calculated peak-to-valley ratios for the first peak and valley as a function of the geometrical parameter B_{02}/B_{01} with the condition $B_{01} + B_{02} =$ constant. Overall increases in the peak-to-valley ratios can be seen as B_{02}/B_{01} is increased for both the 3D–2D and the 2D–1D cases and the peak-to-valley ratio for the 3D–2D case is generally

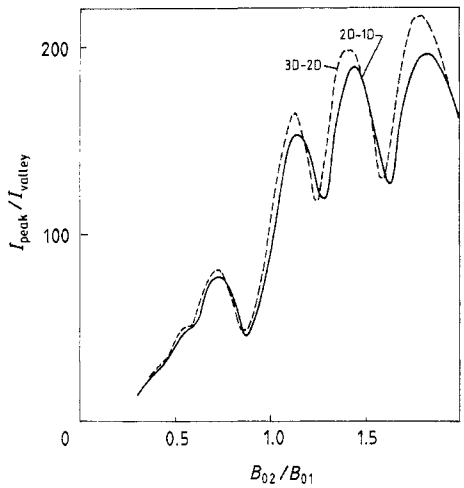

Figure 9. Peak-to-valley ratios as a function of B_{02}/B_{01} with $B_{01} + B_{02} = 40$ Å ($V_0 = 0.5$ eV; $A_0 = 50$ Å; $m_a = m_b = 0.067m_0$; $E_F = 0.005$ eV).

larger than that for the 2D–1D case. So it can be said that we can choose the barrier width ($B_{01} < B_{02}$) to give a larger peak-to-valley ratio which is essential in applications to logic circuits [8].

5. Conclusion

We have presented a solution to the resonant tunnelling problem in the double-barrier structure based upon the exact solution of the Schrödinger equation by use of the Bessel functions. The calculated transmission coefficients here differ from those in [15] in that there is not so much fine structure and there are small deviations in the resonant energies.

The *I–V* characteristics are calculated for both the 3D–2D and the 2D–1D cases. The conclusion is that the shapes of the *I–V* characteristics for these two cases are approximately the same at low Fermi energies. The effect of structural symmetry is considered numerically. The results show that a larger peak-to-valley ratio can be obtained by modulation of the widths of the two barriers.

Acknowledgments

One of the authors (JPP) thanks Professor X X Dai for helpful discussions. The work was supported in part by the Chinese Higher Education Foundation through Grant 2-1985 and in part by the Chinese Science Foundation through Grant 18760723.

References

[1] Tsu R and Esaki L 1973 *Appl. Phys. Lett.* **22** 562
Chang L L, Esaki L and Tsu R 1974 *Appl. Phys. Lett.* **24** 593
[2] Chin R, Holonyak N Jr, Stillman G E, Tang J Y and Hess K 1980 *Electron. Lett.* **16** 467
[3] Capasso F, Tsang W T, Hutchinson A L and Williams G F 1982 *Appl. Phys. Lett.* **40** 38

[4] Capasso F, Mohammed K, Cho A Y, Hull R and Hutchinson A L 1985 *Appl. Phys. Lett.* **47** 420
[5] Smith J S, Chiu L C, Margralit S and Yariv A 1983 *J. Vac. Sci. Technol.* B **1** 376
[6] Capasso F and Kichl R A 1983 *J. Appl. Phys.* **58** 1366
[7] Heiblum M, Thomas D C, Knoedler C M and Nathan M I 1985 *Appl. Phys. Lett.* **47** 1105
[8] Luryi S and Capasso F 1985 *Appl. Phys. Lett.* **47** 1347
[9] Miyazaki S, Ihara Y and Hirose M 1987 *Phys. Rev. Lett.* **59** 125
[10] Sollner T C L G, Goodhue W D, Tannenwald P E, Parker C D and Peck D D 1983 *Appl. Phys. Lett.* **43** 588
[11] Heremans J, Partin D L and Dresselhaus P D 1986 *Appl. Phys. Lett.* **48** 644
[12] Sollner T C L G, Tannenwald P E, Peck D D and Goodhue W D 1983 *Appl. Phys. Lett.* **45** 1319
[13] Luryi S 1985 *Appl. Phys. Lett.* **47** 490
[14] Vassell M O, Lee J and Lockwood H F 1983 *J. Appl. Phys.* **54** 5206
[15] Brennan K F and Summers C J 1986 *J. Appl. Phys.* **61** 614
[16] Ricco B and Azbel Ya 1984 *Phys. Rev.* B **29** 1970
[17] Collins S, Lowe D and Barker J R 1985 *J. Phys. C: Solid State Phys.* **18** L637
[18] Bastard G 1981 *Phys. Rev.* B **24** 5693
[19] Morrow R A and Brownsein K R 1984 *Phys. Rev.* B **30** 678